PNAS RESEARCH ARTICLE | ENGINEERING

Logic-enabled textiles

Anoop Rajappan[a], Barclay Jumet[a], Rachel A. Shveda[a], Colter J. Decker[a], Zhen Liu[a], Te Faye Yap[a], Vanessa Sanchez[b,c], and Daniel J. Preston[a,1]

Edited by John Rogers, Northwestern University, Evanston, IL; received February 9, 2022; accepted July 14, 2022

Textiles hold great promise as a soft yet durable material for building comfortable robotic wearables and assistive devices at low cost. Nevertheless, the development of smart wearables composed entirely of textiles has been hindered by the lack of a viable sheet-based logic architecture that can be implemented using conventional fabric materials and textile manufacturing processes. Here, we develop a fully textile platform for embedding pneumatic digital logic in wearable devices. Our logic-enabled textiles support combinational and sequential logic functions, onboard memory storage, user interaction, and direct interfacing with pneumatic actuators. In addition, they are designed to be lightweight, easily integrable into regular clothing, made using scalable fabrication techniques, and durable enough to withstand everyday use. We demonstrate a textile computer capable of input-driven digital logic for controlling untethered wearable robots that assist users with functional limitations. Our logic platform will facilitate the emergence of future wearables powered by embedded fluidic logic that fully leverage the innate advantages of their textile construction.

assistive devices | fluidic logic | information storage | logic gates | wearable robots

Significance

Despite the tremendous potential of textiles as a robust and versatile medium for building robots and actuators that can be integrated directly into users' clothing, embedded logic controllers made of textiles have not yet been developed, precluding the emergence of smart, fully textile-based robotic wearables. We fill this gap by developing a textile computer capable of pneumatic digital logic, onboard memory, and user interaction and demonstrate its ability to control textile-based assistive devices in response to user commands. Our logic-enabled textiles can be mass produced using existing processes and are resilient enough to withstand everyday use, potentially enabling future generations of comfortable, low-cost, and electronics-free robotic wearables for assisting the nearly one billion people worldwide currently living with disabilities.

Clothing made from textiles has been an integral part of daily human life for millennia, affording comfort, thermoregulation, and protection from the elements (1). Despite their largely passive role in most modern-day clothing, textiles hold great promise as the medium of choice for the next generation of wearable robots and devices due to their proven track record as a soft, flexible, and durable material that conforms and adapts to body shape and movement (2–6). These features are particularly attractive in medical, rehabilitative, and assistive devices, for which textiles can be fashioned into comfortable, lightweight, and low-profile wearables that apply therapeutic forces to the user's body, provide motion assistance, or generate tactile or haptic cues to aid nonverbal or nonvisual communication (6–8). With the concomitant advantages of low cost and mass manufacturability that accompany the use of textiles, such wearable devices have the potential to alleviate functional limitations and facilitate activities of daily living for many of the nearly one billion people in the world (9) who currently live with one or more disabilities.

The current landscape in wearable robotics has witnessed a growing use of textiles in soft actuators intended to function as robotic "muscles" that assist users in physical tasks such as standing up, walking, running, grasping, or lifting objects (2, 6, 7, 10). Such textile-based actuators are powered by means of mechanically driven cables or tendons (11–14), through pouch motors inflated by pressurized fluids (8, 15–19), or by incorporating shape-changing yarns—which respond to thermal, electrical, optical, or chemical stimuli—into the fabric (6). Concurrently, advances in materials and fabrication methods have enabled a range of wearable textile-based sensors that can detect force, pressure, strain, temperature, and moisture (5, 6, 10, 20), as well as fiber-embedded small electronic devices (21). However, even as actuation and sensing elements make steady progress toward fully textile designs, many components critical to their function—traction cables, electrical conductors, and support frames—continue to be constructed of nontextile materials (6). Furthermore, onboard control systems remain heavily reliant on rigid, bulky, or cumbersome components, such as printed circuit boards (PCBs) and arrays of electromechanical valves (22–24); alternatively, some wearables require tethers to an offboard infrastructure that restricts the mobility of the user (25). Fluidic logic represents an attractive approach to control using only soft materials (24, 26–31); however, existing soft valves rely on an inherently three-dimensional architecture and cannot be ported to flexible two-dimensional sheets, precluding their implementation using textiles. Furthermore, the elastomeric construction of these valves prohibits their seamless integration with clothing; the use of nontextile materials adds complexity and failure points, increases the cost of production, and is ultimately incompatible with the end goal of a robust, low-profile, and unified system.

Author affiliations: [a]Department of Mechanical Engineering, Rice University, Houston, TX 77005; [b]John A. Paulson School of Engineering and Applied Sciences, Harvard University, Cambridge, MA 02138; and [c]Wyss Institute for Biologically Inspired Engineering, Boston, MA 02115

Author contributions: A.R., V.S., and D.J.P. designed research; A.R., B.J., R.A.S., C.J.D., Z.L., and T.F.Y. performed research; A.R. analyzed data; and A.R., V.S., and D.J.P. wrote the paper.

The authors declare no competing interest.

This article is a PNAS Direct Submission.

[1]To whom correspondence may be addressed. Email: djp@rice.edu.

This article contains supporting information online at http://www.pnas.org/lookup/suppl/doi:10.1073/pnas.2202118119/-/DCSupplemental.

Published August 22, 2022.

Development of textile-based logic controllers is thus imperative for the emergence of future wearable robots that fully leverage the intrinsic advantages of the textile medium but has been limited by the lack of an approach for embodying intelligence inside a two-dimensional, sheet-based (i.e., textile) architecture.

Here, we address this gap by embedding fluidic digital logic in a fully textile platform for easy integration into robotic wearables. To this end, we developed a textile computer that accepts user input, stores data in memory, and actuates pneumatic assistive devices based on built-in Boolean logic. Our textile logic modules are flexible and lightweight, can be integrated in regular clothing, can withstand tens of thousands of actuation cycles, are robust against washing and rough handling, and can be cascaded successively to implement a wide array of logic functions. We introduce a monolithic fabrication technique for integrated logic circuits based on two-dimensional sheet-based valves; these integrated circuits (ICs) incorporate multiple pneumatic push buttons, valves, resistors, and their interconnections and are formed from stacked textile sheets using scalable and cost-effective processes. Our goal is to enable a unified architecture that tightly integrates various textile-based input devices, logic controllers, and actuators all powered by pressurized air (Fig. 1*A*), in a framework that embodies information processing as a material property (32, 33); such an architecture would be particularly well-suited for wearable robots because of its passive safety, unobtrusive form factor, inherent conformability, and ability to exert usable levels of force required in assistive and therapeutic applications (6, 8). The construction and characteristics of our textile logic platform are detailed in the subsequent sections.

Results and Discussion

Building a Textile Logic Element. Analogous to digital electronics, we built our fluidic logic circuits by combining elementary logical units that are, at a foundational level, textile inverters or NOT gates. Each inverter, in turn, consists of a pneumatic switch or relay (analogous to a field-effect transistor) coupled with an output pull-down resistor; this architecture resembles electronic inverters of the p-channel metal-oxide-semiconductor (or PMOS) logic family (28, 31, 34). The inverter (Fig. 1 *B* and *C* and *SI Appendix*, Movie S1) has three pneumatic connections, as follows: a supply (or enable) port, an input port, and an output port. The enable port receives compressed air at a constant supply pressure P_S, typically 50 kPa gauge, which is adequate for operating most assistive actuators directly (6) (the inverter is however capable of functioning as intended at pressures up to 100 kPa; *SI Appendix*, Fig. S1). Insofar as our textile logic platform employs pneumatic signals, we specify logic levels based on air pressure; we define logical high (or binary 1) as pressure P in the range $0.8 \leq P/P_S \leq 1$ and logical low (or binary 0) as near atmospheric pressure in the range $0 \leq P/P_S \leq 0.1$. We built our devices by heat sealing stacked layers of nylon taffeta fabric coated on one side with a layer of thermoplastic polyurethane (TPU), which renders the textile impermeable and provides robust and gas-tight interlayer adhesion (19, 35) (*SI Appendix*, Fig. S5). Heat-sealable fabrics with thermoplastic coatings are readily available commercially, and the stacked layer assembly of such fabrics is a well-established process in the textile industry for the rapid and low-cost production of textile laminates at scale (36).

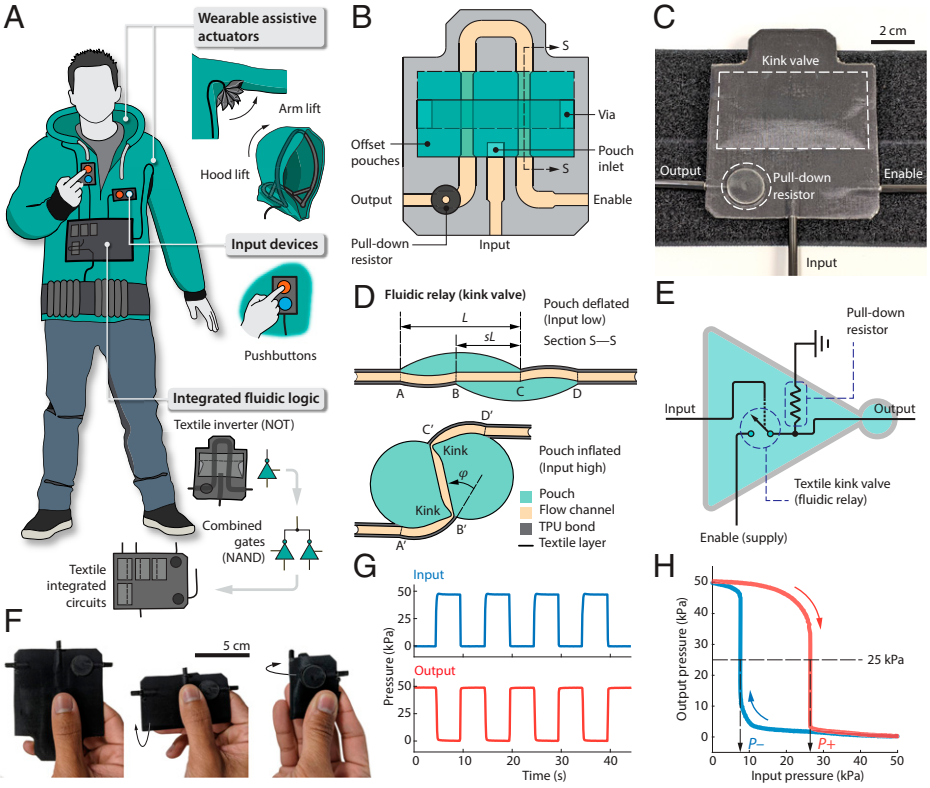

Fig. 1. Pneumatic logic built from textile inverters. (*A*) Schematic overview of a wearable assistive robot that integrates textile actuators, input devices, and control units (built from inverters). (*B*) Internal layout of the textile inverter. (*C*) External features of the device after assembly. (*D*) Operation of the kink valve, showing the kink angle ϕ. The flow channel ABCD deforms into the kinked configuration A′B′C′D′ when the input pouch is inflated. (*E*) Equivalent pneumatic circuit of the inverter, consisting of a normally open fluidic relay (kink valve) coupled to a pull-down resistor. (*F*) The inverter folded in half and then into quarters to show its flexibility. (*G*) Experimental input and output pressure traces, illustrating the switching action of the inverter and its operation as a NOT gate. (*H*) Experimentally measured switching hysteresis of a typical inverter device, showing the forward (P_+) and reverse (P_-) threshold pressures.

The key component of the textile inverter is a pneumatic relay (i.e., a normally open fluidic valve) that isolates the supply port from the output when the input port is pressurized. Traditionally, soft valves in fluidic logic have adopted one of two broad design paradigms, which we call "pinch" and "kink" valve designs. Pinch valves, such as the microfluidic Quake valve (37), directly employ fluid pressure in the control line to deform the flexible wall of an adjoining soft channel and thereby restrict flow in the output line. Although simple in construction, these valves typically entail a drop in fluid pressure between the control and output signals, limiting the ability of gates to be cascaded successively. On the other hand, kink valves exert axial or transverse forces to induce buckling of a soft channel, producing a kink that occludes flow (27–29, 38). This elastic-instability-driven mechanism permits switching of output pressures larger than that of the input signal and yields a sharp and hysteretic on-off transition of the valve (27, 38). Inspired by three-dimensional kink valves that have been successfully deployed for fluidic logic control of soft robots (28–30), we sought to develop an analogous two-dimensional architecture for kink valves that would enable logic gates to be embedded in sheet-based materials such as textiles. However, in contrast to these prior three-dimensional approaches—which include elastomeric components that can exert both tensile and compressive forces due to their material and structural properties—flexible sheets effectively support only tensile loads and readily buckle under in-plane compression. With this constraint in mind, we achieved a reliable valve design by sandwiching the main flow channel (which runs from the supply to the output port) between a pair of inflatable pouches that connect to the input port (Fig. 1*B*); the pouches are linked by pneumatic vias cut into the channel-bearing middle layer, and they inflate (or deflate) in tandem when the input goes high (or low). The top and bottom pouches are offset parallel to the channel and overlap for a distance sL, where L is the width of each pouch; when inflated, the two pouch motors exert a bending torque along the hinge lines B and C, which folds the middle layer into a Z-shape to produce two kinks in each leg of the flow channel (Fig. 1*D*). The maximum fold angle ϕ at the four kink points (attained on full inflation of the pouch walls into circular arcs) may be derived geometrically and is given by $\sin\phi = x$, where $x > 0$ solves the transcendental equation

$$x = \sin\left(\frac{2-s}{s}x\right). \qquad [1]$$

A detailed derivation of this result is included in *SI Appendix, Methods*. The theoretical angle predicted by Eq. **1** is in excellent agreement with the experimentally observed kink angles in our textile devices (Fig. 2), which we measured by cross-sectioning pouches of different overlaps after fixing them in silicone elastomer for visualization. For overlap fractions $s < 0.78$ (regime I in Fig. 2), textile layers in the overlapping region experience tensile loading when the pouches are pressurized, which is a stable configuration that results in kinking of the flow channel without buckling. When the overlap s exceeds 0.78, Eq. **1** predicts kink angles $\phi > 90°$ (regime II); in practice, however, the now-compressive loading from the pouch walls causes buckling of the compliant channel, a largely stochastic process with no certainty of producing kinks (Fig. 2*E*). Our analysis thus suggests a useful guideline for ensuring the reliable operation of kink valves made of compliant sheets (such as textiles); pouches must be designed with an overlap below 78% to maintain axial tension in the channel-bearing layer. An overlap of 50% ($s = 0.5$), for example, yielded reliable kinking with a fold angle of $\phi = 49°$ (Fig. 2 *A* and *C*), which proved sufficient to prevent airflow through the channel at pressures up to 100 kPa; we therefore designed all our textile valves with pouches offset to a 50% overlap.

Insofar as the kink valve merely cuts off the output channel from the supply port, the output pressure "floats" unless an exhaust pathway is provided downstream of the valve via a fluidic pull-down resistor. Although the canonical fluidic resistor is a long, thin, and often serpentine channel, we eschewed this design for various practical reasons, such as: precise alignment of layers required during fabrication, the need for tight tolerances on channel width, and the susceptibility of narrow channels to kink under even mild flexion of the device. Instead, we developed a porous annular resistor, cut from a 1.6-mm-thick sheet of flexible, open-cell polyurethane foam, and bonded permanently to the exterior of the inverter by an interlayer of heat sealable TPU (Fig. 1*C* and *SI Appendix*, Fig. S14). A circular via admits air from the output channel into the center of the annulus, from where it exhausts radially outward through the body of the resistor. The use of foam enables a soft, compliant, and compact resistor design that is largely unaffected by flexion; its fluidic resistance R, computed using Darcy's law, is given by

$$R = \frac{R_S}{2\pi}\ln\left(\frac{r_2}{r_1}\right) \qquad [2]$$

where r_1 and r_2 are the inner and outer radii of the annulus, and R_S is an effective "sheet resistance" of the foam, which is a function of its thickness and permeability as well as the viscosity of the working fluid (air). As in electronic transistor-resistor logic, appropriate sizing of the pull-down resistor entails a trade-off between inverter response time and leakage flow; a small resistance enables a fast transition of the output from high to low, whereas a large resistance minimizes wastage of compressed gas through the resistor when the output is high. For our textile inverters, we sized the pull-down resistors to yield output switching times of 1 s or less in multiple-inverter cascades. Further details on resistor design and characterization are included in *SI Appendix, Methods*.

Fig. 1*E* shows the equivalent pneumatic circuit of the textile inverter, comprising a normally open fluidic relay (kink valve) coupled to an output pull-down resistor. Fig. 1*G* shows the inverter functioning as a fluidic NOT gate; with the enable port set to high, a low-pressure input signal yields a high-pressure output signal and vice-versa. In Fig. 1*H*, the output pressure of the inverter is traced as the input pressure is ramped from zero to P_S and then back to zero. The nonlinear behavior of the kink valve manifests as hysteresis in the inverter's transfer curve, with unequal forward (P_+) and reverse (P_-) switching thresholds (defined, respectively, as the input pressure at which the output falls below, or rises above, $P/P_S = 0.5$). The hysteretic output of our textile inverter resembles that of an inverting Schmitt trigger and confers similar immunity to low-amplitude noise in the input signal (27, 28, 34).

Realizing Modular Logic and Textile-Based Memory. Having built a functional textile-based inverter, we next assembled digital logic circuits by combining multiple inverters in series and parallel configurations; for example, Fig. 3*A* shows a binary NAND gate built using two textile inverters. In this modular configuration, inverters are mounted using hook-and-loop fasteners to permit easy removal and repositioning, and connections between them are "wired" using flexible polyurethane tubing. The same set of inverters can be rewired in multiple ways to realize distinct

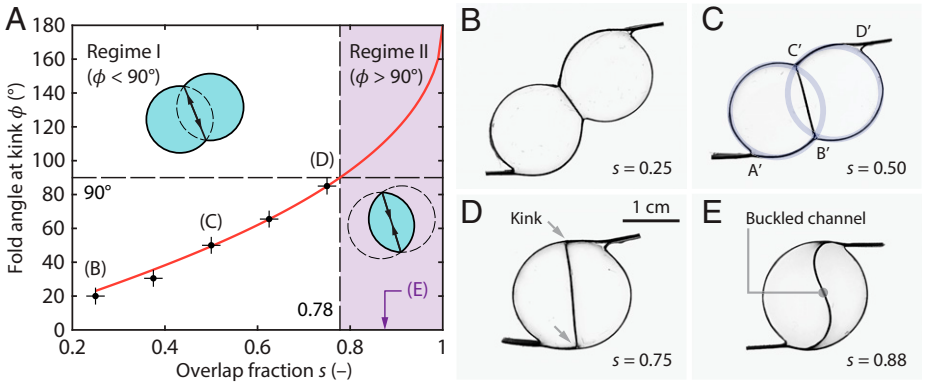

Fig. 2. Architecture of the sheet-based pneumatic kink valve. (*A*) The kink angle ϕ as a function of the pouch overlap *s*; the red curve represents the theoretical angle predicted by Eq. **1**, and the data markers denote experimentally measured angles (averaged over at least three replicate measurements). (*B*–*E*) Representative cross sections of offset pouches of increasing overlap, displaying the internal geometry of the middle layer. The experimentally measured kink angles plotted in *A* were inferred from these images by fitting circles to the pouch walls, as shown with an overlay in *C*. (*E*) Shows overlapping pouches with *s* = 0.88, for which buckling of the channel resulted in a smooth profile devoid of kinks.

logic functions; as an illustration, we built a unary logic buffer and a binary NOR gate (*SI Appendix*, Fig. S2) by reconfiguring the same inverter pair in Fig. 3*A* and further built binary AND and OR gates by adding a third inverter module (*SI Appendix*, Fig. S3). The ability to construct NAND and NOR gates ensures, in principle, the functional completeness of our textile logic system; any Boolean function may be reduced to a network composed of either one of these gates (28, 39). We thus envision a modular logic platform—akin to an electronic breadboard—composed of textile inverters affixed to regular clothing and configured on-the-fly to program specific logical operations as desired by the user. Insofar as our logic circuits emulate a simple digital computer, we characterized the speed of our pneumatic gates by measuring signal propagation delay and frequency response; the delay (for a fan-out of one) was ∼0.6 s per inverter, and switching speeds exceeding 1 Hz were achieved (*SI Appendix*, Figs. S15 and S16; experimental details included in *SI Appendix*, *Methods*). We anticipate that the relatively fast response time of our logic circuits will enable responsive user-driven control of many current and future wearable pneumatic actuators.

In addition to the combinational logic circuits described above, we also used textile logic modules to implement asynchronous, input-driven sequential logic; specifically, we built a pneumatic set-reset (SR) latch from a pair of cross-coupled inverters, as shown in Fig. 3*B*. The latch has two active-high inputs, S and R, which drive the output Q high or low, respectively; when both inputs are inactive (low), the output state persists. A single SR latch thus contributes one bit of textile-based volatile memory capable of storing an internal state of the system (39). For example, in our subsequent demonstration of a prototype wearable robot, we use this 1-bit memory to store the current state—inflated or deflated—of an assistive pneumatic actuator and to switch its state in response to user input. For more complex logic controllers, we anticipate that many such textile latches can be arrayed to create multibit registers. The ability to realize both combinational and sequential logic using

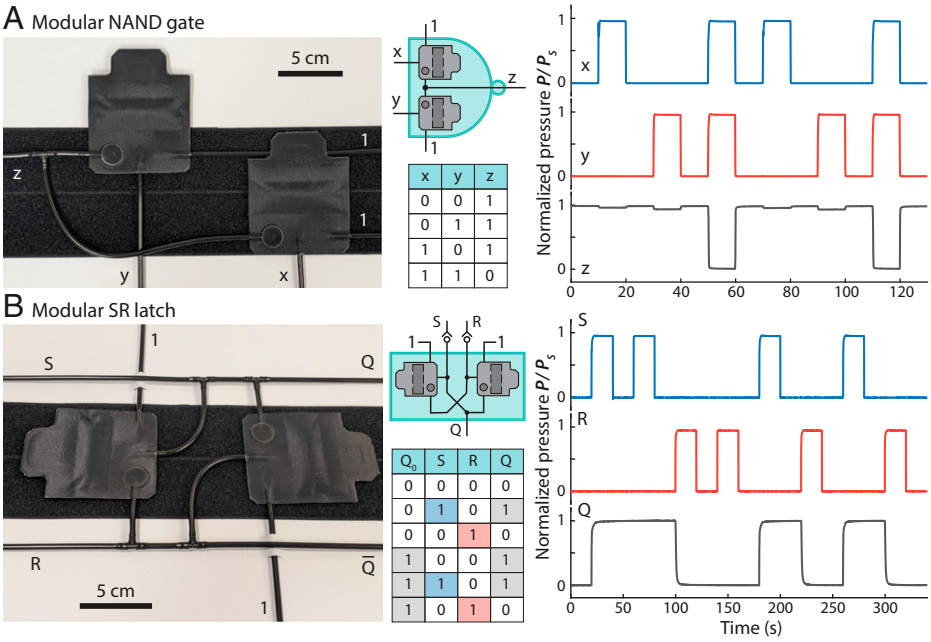

Fig. 3. Modular logic circuits assembled from two textile inverter units. (*A*) A binary NAND gate, along with its logic circuit, truth table, and experimentally measured pressure traces. (*B*) An SR latch, along with its logic circuit, state-transition table, and experimentally measured pressure traces for various state-input combinations. The combination S = R = 1 is not a valid input for operating the latch. Full pneumatic circuit diagrams for all modular logic gates are included in *SI Appendix*, Fig. S17.

only textile inverters indicates that any soft controller that emulates a finite-state machine may, in principle, be built entirely out of textiles using our pneumatic logic architecture (39).

Designing a Textile IC Capable of User Interaction. To enable our textile controllers to accept user input, we designed pneumatic pushbutton valves (resembling momentary electronic switches) by bonding colored circular foam pads over textile input channels to the controller (Fig. 4*A*). With the upstream of the valve connected to the air supply line, the channel remains open by virtue of internal gas pressure and the valve output is normally high. The user sends an active-low signal to the controller by depressing the pad with a finger, constricting airflow through the channel below; a foam resistor placed downstream of the valve then pulls the output low. Releasing pressure on the pad reopens the channel, and the pushbutton and resistor assembly thus behaves as a normally open, momentary action fluidic switch (Fig. 4*D* and *SI Appendix*, Fig. S8). We sized the button and the channel underneath to limit the valve actuation force to 30 N or less, aiming to keep our device accessible to users with limitations in finger force (*SI Appendix*, *Methods*).

Taking a step forward from the modular architecture, we next integrated the various input, logic, and memory elements described previously into a unified textile-based wearable controller, analogous to small-scale integration of transistor-based electronics into monolithic ICs or microchips (39). To enable the input-driven control of actuators, we employed a pair of color-coded pushbutton valves to drive the S and R inputs of an SR latch, utilizing an intermediate layer of inverters to convert the output of each button from active-low to active-high (Fig. 4*B*). Our textile IC thus packages two pushbuttons, four pneumatic kink valves, and four pull-down resistors into a compact form factor for facile integration into clothing (Fig. 4*C*); furthermore, external tubing between components is replaced by internal channels that run between textile layers. To achieve a tight layout with minimal footprint, we routed internal channels along three "pneumatic layers," akin to conductive layers on a multilayer PCB; in this configuration, channels cross each other in two dimensions as traces do on a PCB, and vias enable connections between channels on different layers. As in the case of electronic chips, this integrated design facilitates a rapid and efficient fabrication pipeline whereby all internal features and connections are formed from stacked textiles in a one-step heat sealing process (*SI Appendix*, Figs. S6 and S7). Fig. 4*E* shows the textile IC responding to tactile input from the user; the latched output Q goes high or low, respectively, when the set and reset buttons are pressed, and these output values persist between user interactions.

Building Wearable, Logic-Enabled Textile Robots. Finally, to demonstrate the capabilities of our textile logic platform, we built wearable assistive robots by integrating the logic controller above with two pneumatic actuators, namely: an arm-lift that assists users in abduction (lateral elevation) of the arm and a hood-lift to don and doff the hood of a jacket for thermoregulation. Both actions involve lifting the arm to or above the level of one's shoulders and can be challenging for users with functional limitations of the upper body. For context, in the United States alone, about 30 million people live with an upper body functional limitation; the most common limitation is difficulty lifting a 10-pound object, which affects 10.2% of adults, or about 25 million people (40).

Both the arm-lift and hood-lift robots were built by heat sealing textile layers and designed to be integrated into the user's clothing. The arm-lift actuator comprises a series of six inflatable pouches attached securely to the user's clothing under the shoulder joint; when pressurized, the pouches exert force on the upper arm, generating a lifting torque that helps the user raise their arm or a weight they intend to carry (41). To construct the hood-lift, we built a pair of inflatable textile collars to support the hood at the opening and neckline. On actuation, textile bellows affixed to the collar hinges draw the hood

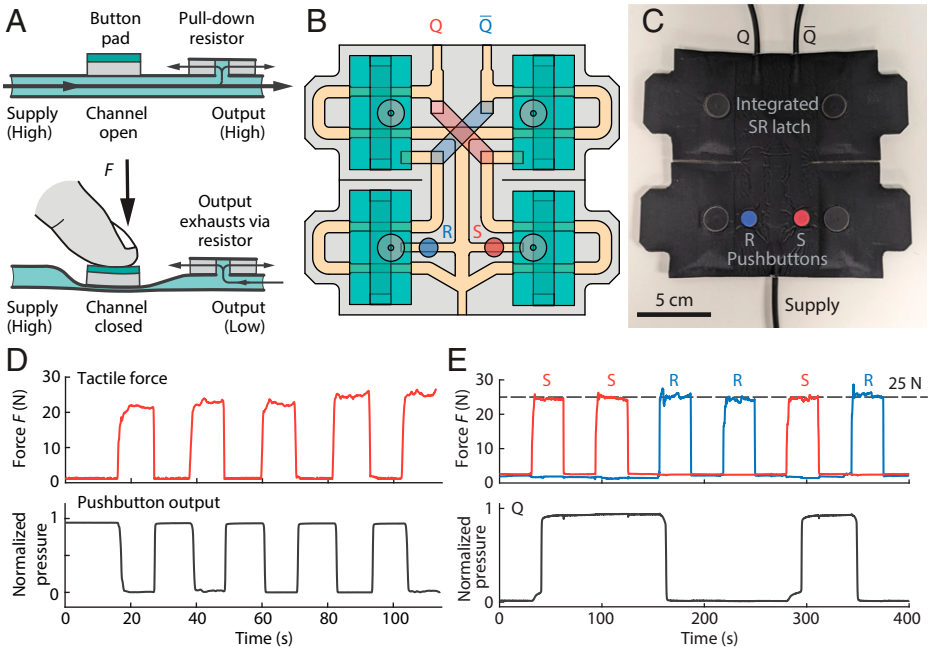

Fig. 4. Textile ICs for user-driven logic control. (*A*) Actuation mechanism of the pushbutton valve. (*B*) Internal layout of the textile controller, showing channels, pouches, and vias that enable latch operation in response to user input. A complete pneumatic circuit diagram of the controller is included in *SI Appendix*, Fig. S17. (*C*) Photograph of the heat-sealed textile IC with integrated resistors and pushbuttons. (*D*) Active-low output generated by a single pushbutton in response to finger presses by the user. (*E*) Experimental traces showing user-applied force on the controller pushbuttons and the corresponding change in the latch output Q.

over the user's head; afterward, a pair of elastic textile "springs" retract the hood to its doffed position when the actuators are depressurized. To drive either actuator in response to user commands, we linked their pneumatic inputs to the output $\bar{Q}$ of the textile controller through an intermediate textile inverter (operating as a NOT gate); the inverter pneumatically isolates the logic circuit from the large fluidic capacitance of the actuator, enabling the latch to function at normal speed (Fig. 5*A*). To permit untethered operation of our robot, we employed a portable compressed gas cartridge to power both the controller and the actuators. Our assistive robot is capable of standalone operation provided a source of compressed gas is available; this could in the future be a wearable textile tank that is refilled periodically or an integrated energy-harvesting device that generates pressurized gas onboard (26, 41–45).

Fig. 5 *B* and *C* show the two assistive actuators responding to button presses by a user (full sequences are included as *SI Appendix*, Movies S2 and S3); the actuators inflate when the user presses the set button on the controller, which raises the arm or draws the hood over the user's head. The devices remain pressurized until the reset button is pressed, which triggers their deflation through the inverter's pull-down resistor, thus lowering the arm or retracting the hood to its undeployed configuration. The plot in Fig. 5*C* shows the raised hood conserving body heat during a light breeze, thereby lending thermoregulatory assistance to the user.

Durability of the Textile Logic Platform. To ensure that our wearable logic platform meets the durability requirements for everyday use, we tested our inverters under accelerated wear conditions to simulate the aging, fatigue, and rough handling expected during long-term service (Fig. 6 and *SI Appendix*, Movie S4). The inverter remained operational after 20,000 actuation cycles (Fig. 6*A* and *SI Appendix*, Fig. S9) at the intended working pressure of 50 kPa (and withstood over 10,000 cycles at 100 kPa before failure; *SI Appendix*, Fig. S1). We followed this with a flexion test (repeated folding in half; Fig. 6*B*) and observed no degradation in performance after one million cycles (Fig. 6*C* and *SI Appendix*, Fig. S10). The inverter also remained functional after 20 cycles of machine washing (Fig. 6*D* and *SI Appendix*, Fig. S11) and being run over five times by a midsize pickup truck (Fig. 6*E* and *F* and *SI Appendix*, Fig. S12).

In conclusion, we present a practical framework for embedding fluidic logic inside two-dimensional textile laminates, in a form factor suitable for facile integration into future wearable robots and assistive garments. Our textile-based logic platform supports combinational and sequential logic functions, onboard memory storage, user interaction, and direct interfacing with pneumatic actuators, while retaining many of the inherent advantages of textiles, such as: comfort, durability, conformability, low production cost, and scalable manufacturing. Key aspects of our fluidic logic architecture have direct parallels in digital electronics, enabling cross-domain transfer of knowledge, tools, and proven design principles that currently exist for transistor-based electronic logic circuits. With the further development and optimization of textile materials, fabrication methods, and geometry of internal fluidic pathways, we envision that these logic-enabled textiles will facilitate a future generation of "smart," soft, and electronics-free wearable assistive robots.

Materials and Methods

Fabrication of Textile Logic Devices. To fabricate the textile inverters and the integrated textile logic controller, we first applied an adhesive paper tape (V0821, Vinyl Ease) to mask (i.e., prevent adhesion of) the TPU-coated side of heat-sealable, 70-denier nylon taffeta fabric (Seattle Fabrics). This masked textile sheet was then patterned using a 40-W desktop laser cutter (DF0812-40RW, OMTech Laser) with the mask side facing up to create all six layers of the device; outlines on the paper mask were engraved at 5.0 to 5.6% laser power and 15-mm s^{-1} engraving speed, whereas cuts through the textile layer were made at 7% laser power and 15-mm s^{-1} cutting speed. After manual weeding to remove extraneous regions of the mask, the layers were stacked, vertically aligned, and heat sealed using a benchtop heat press (DK20SP, Geo Knight & Co Inc.) at 200 °C and 40-kPa platen pressure for a duration of 30 s. (*SI Appendix*, Figs. S5–S7 show the individual textile layers of the inverter and

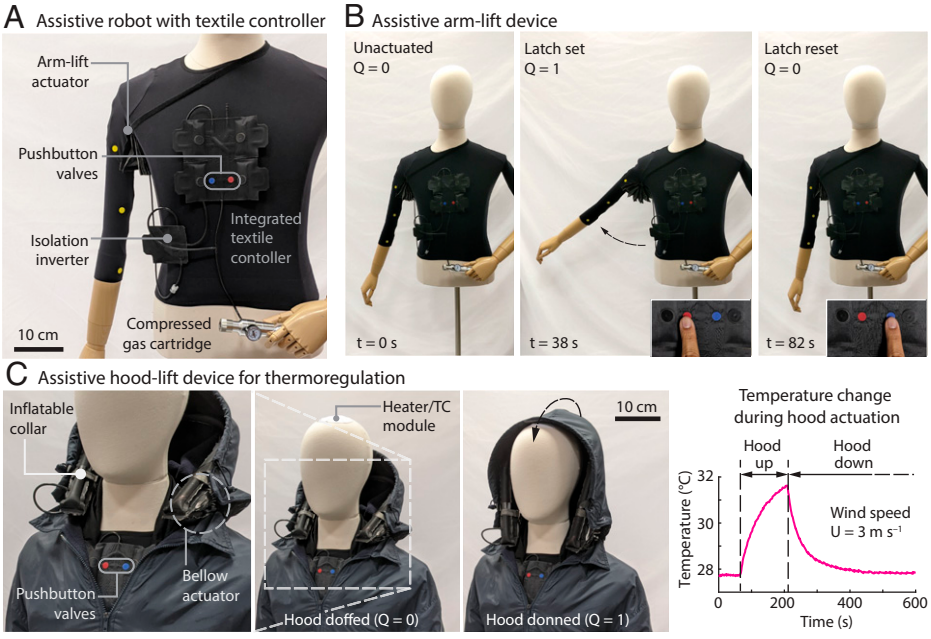

Fig. 5. Controlling wearable assistive robots using textile logic. (*A*) The textile IC configured for controlling a wearable assistive robot. The controller is mounted on the user's garment using hook and loop fasteners and supplied from a portable gas cartridge. (*B*) User-driven operation of the textile-based arm-lift actuator. (*C*) User-driven operation of the textile-based hood actuator. The plot on the right shows an increase in measured skin temperature upon donning the hood in light breeze.

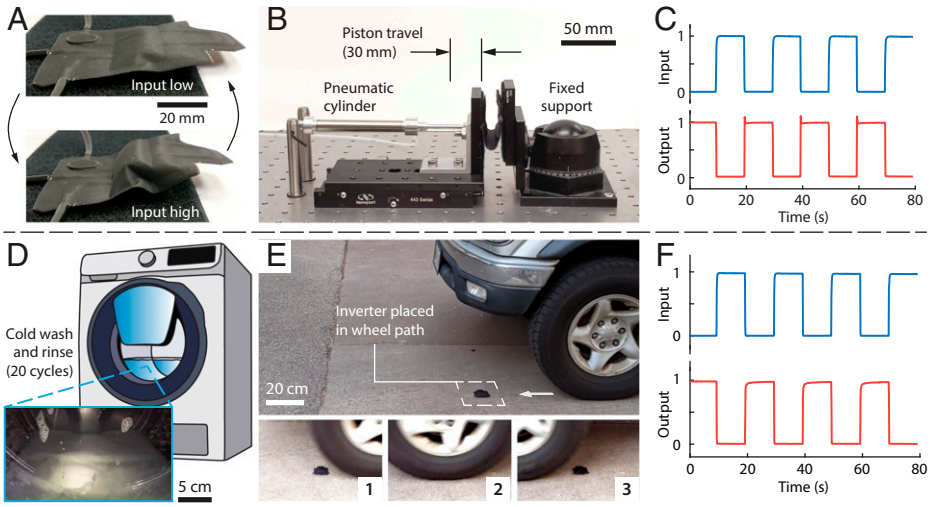

Fig. 6. Accelerated wear and durability tests on the textile inverter. (*A*) Cyclical switching of the textile inverter at 50-kPa supply pressure. (*B*) The inverter being folded repeatedly in half on a bespoke test rig. (*C*) Experimental pressure traces confirming normal functioning of the inverter after 20,000 on-off cycles and one million flex cycles. (*D*) Laundering the inverter in a washing machine. (*E*) The inverter being run over with a pickup truck to simulate rough handling. (*F*) Experimental pressure traces confirming normal functioning of the inverter after 20 wash cycles and being run over 5 times (i.e., 10 passes of the truck wheels).

the integrated controller prior to heat sealing; the vector design files used to pattern these layers are included as *SI Appendix*, Data S1.)

Pull-down resistors were cut from a 1/16-inch-thick sheet of open-cell polyurethane foam (86375K132, McMaster-Carr) using a concentric hollow punch (66004, Mayhew Steel Products Inc.) and thermally bonded to exhaust vias on the device using an interlayer of thin (38-μm) TPU film (Stretchlon 200, Airtech International Inc.). To create pushbutton valves, we used the same technique to attach 10-mm-diameter circular foam pads atop 5-mm-wide pneumatic input channels. The central via of each resistor was sealed at the top by bonding a disk of TPU-coated nylon taffeta, ensuring radial outflow of gas through the foam. Finally, pneumatic ports were attached to the heat-sealed device using two-part epoxy glue (clear epoxy, Gorilla Inc.) to create airtight joints.

Visualization of the Kink Geometry. To obtain measurements of the kink angle shown in Fig. 2, we used a low-shrinkage, translucent, platinum-cured silicone rubber (Ecoflex 00-30, Smooth-On Inc.) to fix pouches in their inflated state for sectioning. Textile pouches with overlap fractions in the range $0.25 < s < 0.88$ were fabricated with dimensions identical to the pouches used in our textile inverters. Liquid prepolymer was injected into the pouches at 80 kPa to simulate actuation with compressed air and subsequently allowed to cure at room temperature for 4 h while still under pressure. Once cured, transverse sections of the filled pouches, each ∼5 mm thick, were prepared by slicing through with a sharp razor and photographed atop a white light-emitting diode backlight. Kink angles were then estimated from the images by fitting circles to the pouch walls, as shown in Fig. 2*C*.

Fabrication of Assistive Actuators. Both the arm-lift and hood-lift actuators were made by heat sealing multiple layers of TPU-coated nylon taffeta fabric (Seattle Fabrics). The arm-lift actuator was built from six inflatable textile pouches that were sewn under the right arm of a close-fitting, long sleeve compression shirt. When pressurized, the pouches exert force on the upper arm, thereby generating a lifting torque that helps the user raise their arm or a weight they intend to carry. To construct the hood-lift, we built a pair of inflatable U-shaped textile collars to support the hood of a regular jacket at the crown and the neckline. We joined the collar legs to form a clamshell and added bellows actuators constructed from the same textile at the hinges, each made of eight inflatable pouches. As the dimensions of the collars exceeded the usable work area of our laser cutter, we divided each collar into multiple tubular segments that were cut separately and then heat sealed together; to create these segments and the two bellows actuators, textile sheets were masked using adhesive paper (DL8511FS, Packzon) and subsequently patterned on a desktop cutting plotter (Cricut Maker 3, Cricut Inc.). The collars of the hood-lift were kept pressurized at 50 kPa during use to impart structural integrity to the tubes and provide support to the hood opening. The bellows were inflated (independently of the collars) to actuate the hinge and pull the hood over the user's head. Strips of elastic fabric (Dritz 1/2-inch braided elastic, Prym Consumer USA Inc.) affixed to the hinges were employed as soft springs to aid the retraction of the hood to its doffed position when the bellows are depressurized.

Pneumatic Testing of Textile Inverters. We fed the supply ports of devices under test with compressed air at 50-kPa gauge pressure, drawn from the building air supply through a diaphragm-type pressure regulating valve (PR364, Parker Hannifin Corporation). For square-wave signals, the input of the inverter was connected to a 50-kPa compressed air supply through a pneumatic solenoid valve (VT307-5DZ1-02N-F, SMC Corporation; *SI Appendix*, Fig. S15). The valve was then switched between supply and exhaust pressures using pulsed digital output from a computer-based data acquisition device (USB-6210, National Instruments). For hysteresis measurements, the input pressure was gradually ramped up to 50 kPa and then back to 0 kPa (keeping the time rate of change of input pressure < 0.5 kPa s^{-1}) by means of an electronic proportional regulator (ITV0010-2BL, SMC Corporation) that, in turn, was controlled using the analog voltage output of a computer-based data acquisition device (USB-6002, National Instruments).

For static pressure measurements and steady-state monitoring of supply and input pressures during tests, we used digital pneumatic pressure gauges (MG1-30-A-9V-R, SSI Technologies Inc.). For transient or dynamic measurements of input and output pressure signals, we used electronic pressure sensors (ADP5151, Panasonic Corporation) in conjunction with an analog voltage acquisition device (USB-6002, National Instruments). Typically, a sampling rate of 10 Hz was employed when recording pressure traces, except during frequency response tests, for which a sampling rate of 20 times the frequency of the input square wave was used. All data acquisition, processing, and plotting routines were implemented as custom scripts in MATLAB (version R2021a, MathWorks Inc.).

Testing of Modular Logic Circuits. To build modular logic circuits, we mounted textile inverter units on a poster board using hook-and-loop fasteners; hook pads were attached to the bottom of each inverter, and loop strips were applied to the poster board to create a "Velcro breadboard" (*SI Appendix*, Figs. S2 and S3). Pneumatic connections between inverter modules were wired using flexible polyurethane tubes (3/32" inside diameter; 5648K231, McMaster-Carr) that were cut to the desired length and push fit onto the inverters' pneumatic ports. All inverters were supplied with compressed air at 50 kPa through a diaphragm-type pressure-regulating valve (R364-02BG, Parker Hannifin Corporation). Input pulses to various logic gates were generated using 3-way push button valves (A11-30-14, Pneumadyne Inc.) that we operated manually; for testing the modular SR latch, we added one-way check valves

(2141N3, McMaster-Carr) downstream of the S and R push buttons to avoid exhausting the cross-coupled output lines when the input signal is low. For all experiments, input and output pressure traces were acquired using electronic pressure sensors (ADP5151, Panasonic Corporation) as described previously.

Measurement of Actuation Force on Tactile Pushbuttons. To measure the force applied on the input pushbuttons of the textile integrated controller, we mounted a force-sensing resistor (FSR 402, Interlink Electronics Inc.) directly beneath each button pad using double-sided adhesive tape. Each sensor, in turn, was wired in series with a 981-Ω axial resistor and a 5.45-V DC source to form a voltage divider circuit (*SI Appendix*, Fig. S8). The transient voltage drop across the two sensors during button presses was recorded using a computer-based data acquisition device (USB-6210, National Instruments), and the resistance $R(t)$ of the sensors as a function of time t was inferred from the measured voltage as

$$R(t) = R_0 \frac{V_0}{V_0 - V(t)}. \quad [3]$$

Here $V(t)$ denotes the output voltage across the force sensor, $R_0 = 981\ \Omega$ is the known value of the series resistor, and $V_0 = 5.45$ V is the input voltage supplied by the DC source. To convert the resistance of the sensor into a corresponding value of the applied force, we used an empirical force vs. resistance curve of the form

$$\log_{10} F(t) = \frac{a \log_{10} R(t) + b}{\log_{10} R(t) + c}, \quad [4]$$

where the force $F(t)$ is expressed in newton, the resistance $R(t)$ is expressed in ohm, and the coefficients $a = -0.4363$, $b = 3.239$, and $c = -1.399$ were determined by least squares regression to the experimentally measured response curve of the sensor. To ascertain this response curve, we employed a universal testing machine (68SC-2, Instron) to perform controlled loading of the sensor while measuring its resistance using a digital multimeter (26 Series III multimeter, Fluke Corporation); a silicone rubber block (of size 31 mm by 50 mm) served to distribute the force evenly across the sensor face and improve the resolution of force measurements–obtained using a 1-kN load cell–after appropriate scaling by the ratio of sensor to block area. A schematic of the experimental setup used for sensor calibration is shown in *SI Appendix*, Fig. S8.

Testing the Wearable Assistive Robot. To assemble the logic-enabled wearable robot, we attached the integrated textile controller and the inverter module (acting as the pneumatic isolator) to the front of the user's clothing by means of hook-and-loop fasteners. Pneumatic connections between the gas source, controller, inverter, and actuator were all wired using flexible polyurethane tubing (3/32″ inside diameter; 5648K231, McMaster-Carr). For tests involving the arm-lift actuator, we used a mannequin (JF-33M01ARM, Roxy Display Inc.) with a freely rotating shoulder joint to preclude the inadvertent application of muscular effort that could result from testing on a human user. Compressed gas at ∼40-kPa pressure was supplied from a portable, single-use carbon dioxide cartridge (GF-CO_2-25G-5PK, Gorilla Force) fitted with a miniature pressure regulator; each cartridge contained 25 g of gas and weighed ∼92 g when full.

For testing the hood-lift assistive robot, we again used disposable cartridges (17559, Fluval) fitted with a miniature regulator (NS-BMR-L, Kegco) to supply pressurized gas at 7 psi (48 kPa) to the actuator and logic devices; each single-use cartridge contained 95 g of liquified carbon dioxide. The bellows actuators were inflated or deflated by means of the textile controller to raise or lower the hood, respectively, whereas the support collars were kept pressurized throughout the full duration of the test. To demonstrate the thermoregulatory function of the hood-lift, we used a small resistive heater to simulate body heat flux through the scalp and measured the change in "skin temperature" when donning and doffing the hood in a light breeze. To this end, we attached a flexible thin-film heater (2″ diameter; Omegalux KHR-2/10, Omega Engineering Inc.) and a T-type thermocouple atop the mannequin's head using polyimide tape (7708-10 Kapton 2″ tape, Electron Microscopy Sciences); we then pasted a disk of adhesive paper (DL8511FS, Packzon) over the heater-and-thermocouple assembly to secure it firmly to the scalp. The heater was supplied with 14.0-V DC from a constant voltage source (DY-SPS3010W, Kungber), and its surface temperature, as measured by the thermocouple, was recorded using a computer-based data acquisition device (USB-TC01, National Instruments). To simulate the effect of wind chill, we placed an air-circulating fan (HT-900, Honeywell; medium speed setting) about 3 ft away from the mannequin; we measured the resulting wind speed to be $U = 3.0$ m s^{-1} using a metal vane anemometer (407113, Extech Instruments). A wind of this speed would be categorized as a "light breeze," or Force 2 on the Beaufort wind scale (http://www.weather.gov/mfl/beaufort). Under these test conditions, the power dissipated by the heater was 0.38 W, corresponding to a surface heat flux of 187 W m^{-2}; the steady-state skin temperatures measured with the hood raised and lowered were ∼36 °C and 28 °C, respectively.

When testing the arm-lift and hood-lift actuators, we observed a longer time delay for latch operation due to the additional fluidic resistance imposed by the small diameter flexible tubing used to create pneumatic connections between the controller, the isolation inverter, and the actuators; this delay could be mitigated by using tubing of a larger diameter. In *SI Appendix*, Movies S2 and S3, this increased time lag resulted in a slightly longer button press required for operating the textile controller.

Accelerated Wear and Durability Tests. For accelerated wear tests, we connected the textile inverter to 50-kPa supply pressure and repeatedly switched the input on and off at 1-s intervals using a solenoid valve, for a total of 20,000 cycles. Hysteresis measurements were performed at intermediate checkpoints to monitor changes in device performance with cycling (*SI Appendix*, Fig. S9). Afterward, we tested the same inverter module under repeated flexion, utilizing a bespoke test rig (a linear slide driven by a reciprocating pneumatic cylinder; Fig. 6*B*) to fold the device in half once per second for a total of one million cycles. Once again, hysteresis measurements were performed at various points during the test and showed no discernible change in switching performance (*SI Appendix*, Fig. S10).

Before washing the inverter, we sealed off its pneumatic ports to prevent the ingress of water into the pouches and internal flow channels (*SI Appendix*, Fig. S11). The inverter was then placed inside a mesh bag and subjected to 5 consecutive wash-and-rinse cycles inside a front-load washing machine (model WF45R6100AW/US, Samsung Electronics Co. Ltd.); we used a cold-water cycle and added the requisite amount of laundry detergent (Tide Free and Gentle, Procter & Gamble). After drying the device in air, we performed hysteresis tests to evaluate degradation in switching performance caused by washing. The above process was repeated 4 times until a total of 20 wash cycles were achieved (*SI Appendix*, Fig. S11).

As a final durability test, we ran the inverter (the same unit used in the wash test above) over with a pickup truck (2002 Toyota Tacoma, 4WD Xtracab 4ECT; curb weight: 1,606 kg) 5 times (i.e., 10 passes of the wheel) and measured its performance afterward (*SI Appendix*, Fig. S12). The inverter remained functional and showed no significant change in either the forward or reverse switching thresholds.

Data Availability. All study data are included in the article and/or supporting information.

ACKNOWLEDGMENTS. We thank Marquise D. Bell and Nathaniel Fino for assistance with videography. Scanning electron micrographs were obtained at the Shared Equipment Authority at Rice University. A.R. acknowledges support from the Rice University Academy of Fellows. B.J. acknowledges support from the NSF Graduate Research Fellowship. V.S. acknowledges support from the National Defense Science and Engineering Graduate fellowship and from the GEM fellowship through the National GEM Consortium. This material is based upon work supported by the NSF under Grant no. CMMI-2144809 and Grant no. DMR-2138020 and the NSF Graduate Research Fellowship Program under Grant no. 1842494.

1. J. Harris, *Textiles, 5,000 Years: An International History and Illustrated Survey* (H. N. Abrams, 1993).
2. N.-K. Persson, J. G. Martinez, Y. Zhong, A. Maziz, E. W. H. Jager, Actuating textiles: Next generation of smart textiles. *Adv. Mater. Technol.* **3**, 1700397 (2018).
3. G. Chen, Y. Li, M. Bick, J. Chen, Smart textiles for electricity generation. *Chem. Rev.* **120**, 3668–3720 (2020).
4. J. Shi *et al.*, Smart textile-integrated microelectronic systems for wearable applications. *Adv. Mater.* **32**, e1901958 (2020).

5. J. Xiong, J. Chen, P. S. Lee, Functional fibers and fabrics for soft robotics, wearables, and human-robot interface. *Adv. Mater.* **33**, e2002640 (2021).
6. V. Sanchez, C. J. Walsh, R. J. Wood, Textile technology for soft robotic and autonomous garments. *Adv. Funct. Mater.* **31**, 2008278 (2021).
7. C. Thalman, P. Artemiadis, A review of soft wearable robots that provide active assistance: Trends, common actuation methods, fabrication, and applications. *Wearable Technol.* **1**, e3 (2020).
8. P. H. Nguyen, W. Zhang, Design and computational modeling of fabric soft pneumatic actuators for wearable assistive devices. *Sci. Rep.* **10**, 9638 (2020).
9. World Health Organization, "World Report on Disability 2011" (WHO, 2011). https://www.who.int/publications/i/item/9789241564182.
10. B. Jumet, M. D. Bell, V. Sanchez, D. J. Preston, A data-driven review of soft robotics. *Adv. Intell. Syst.* **4**, 2100163 (2021).
11. A. T. Asbeck, S. M. M. De Rossi, K. G. Holt, C. J. Walsh, A biologically inspired soft exosuit for walking assistance. *Int. J. Robot. Res.* **34**, 744–762 (2015).
12. N. Li *et al.*, Bio-inspired upper limb soft exoskeleton to reduce stroke-induced complications. *Bioinspir. Biomim.* **13**, 066001 (2018).
13. J. Kim *et al.*, Reducing the metabolic rate of walking and running with a versatile, portable exosuit. *Science* **365**, 668–672 (2019).
14. N. Li *et al.*, Bioinspired musculoskeletal model-based soft wrist exoskeleton for stroke rehabilitation. *J. Bionics Eng.* **17**, 1163–1174 (2020).
15. A. R. Mettam, "Inflatable Servo Actuators" (C. P. No. 671, Ministry of Aviation, Aeronautical Research Council, London, 1964).
16. Y.-L. Park, J. Santos, K. G. Galloway, E. C. Goldfield, R. J. Wood, "A soft wearable robotic device for active knee motions using flat pneumatic artificial muscles." in *2014 IEEE International Conference on Robotics & Automation (ICRA)* (IEEE, 2014), pp. 4805–4810.
17. P. Polygerinos, Z. Wang, K. C. Galloway, R. J. Wood, C. J. Walsh, Soft robotic glove for combined assistance and at-home rehabilitation. *Robot. Auton. Syst.* **73**, 135–143 (2015).
18. S. Sridar, Z. Qiao, N. Muthukrishnan, W. Zhang, P. Polygerinos, A soft-inflatable exosuit for knee rehabilitation: Assisting swing phase during walking. *Front. Robot. AI* **5**, 44 (2018).
19. V. Sanchez *et al.*, Smart thermally actuating textiles. *Adv. Mater. Technol.* **5**, 2000383 (2020).
20. G. Loke, W. Yan, T. Khudiyev, G. Noel, Y. Fink, Recent progress and perspectives of thermally drawn multimaterial fiber electronics. *Adv. Mater.* **32**, e1904911 (2020).
21. G. Loke *et al.*, Digital electronics in fibres enable fabric-based machine-learning inference. *Nat. Commun.* **12**, 3317 (2021).
22. D. Rus, M. T. Tolley, Design, fabrication and control of soft robots. *Nature* **521**, 467–475 (2015).
23. A. Rajappan, B. Jumet, D. J. Preston, Pneumatic soft robots take a step toward autonomy. *Sci. Robot.* **6**, eabg6994 (2021).
24. K. McDonald, T. Ranzani, Hardware methods for onboard control of fluidically actuated soft robots. *Front. Robot. AI* **8**, 720702 (2021).
25. S. I. Rich, R. J. Wood, C. Majidi, Untethered soft robotics. *Nat. Electron.* **1**, 102–112 (2018).
26. M. Wehner *et al.*, An integrated design and fabrication strategy for entirely soft, autonomous robots. *Nature* **536**, 451–455 (2016).
27. P. Rothemund *et al.*, A soft, bistable valve for autonomous control of soft actuators. *Sci. Robot.* **3**, eaar7986 (2018).
28. D. J. Preston *et al.*, Digital logic for soft devices. *Proc. Natl. Acad. Sci. U.S.A.* **116**, 7750–7759 (2019).
29. D. J. Preston *et al.*, A soft ring oscillator. *Sci. Robot.* **4**, eaaw5496 (2019).
30. D. Drotman, S. Jadhav, D. Sharp, C. Chan, M. T. Tolley, Electronics-free pneumatic circuits for controlling soft-legged robots. *Sci. Robot.* **6**, eaay2627 (2021).
31. S. Song, S. Joshi, J. Paik, CMOS-inspired complementary fluidic circuits for soft robots. *Adv. Sci. (Weinh.)* **8**, e2100924 (2021).
32. H. Yasuda *et al.*, Mechanical computing. *Nature* **598**, 39–48 (2021).
33. R. L. Truby, Designing soft robots as robotic materials. *Accounts Mater. Res.* **2**, 854–857 (2021).
34. P. Horowitz, W. Hill, *The Art of Electronics* (Cambridge University Press, 2021).
35. H. D. Yang, A. T. Asbeck, A layered manufacturing approach for soft and soft-rigid hybrid robots. *Soft Robot.* **7**, 218–232 (2020).
36. I. Jones, "The use of heat sealing, hot air and hot wedge to join textile materials" in *Joining Textiles*, I. Jones, G. K. Stylios, Eds. (Woodhead Publishing, 2013), pp. 355–373.
37. M. A. Unger, H.-P. Chou, T. Thorsen, A. Scherer, S. R. Quake, Monolithic microfabricated valves and pumps by multilayer soft lithography. *Science* **288**, 113–116 (2000).
38. K. Luo, P. Rothemund, G. M. Whitesides, Z. Suo, Soft kink valves. *J. Mech. Phys. Solids* **131**, 230–239 (2019).
39. M. M. Mano, *Digital Logic and Computer Design* (Prentice-Hall International, 1979).
40. D. M. Taylor, "Americans with Disabilities: 2014" (US Department of Commerce, 2018).
41. R. A. Shveda *et al.*, A wearable textile-based pneumatic energy harvesting system for assistive robotics. *Sci. Adv.* 10.1126/sciadv.abo2418, in press.
42. T. Wang, W. Song, S. Zhu, Analytical research on energy harvesting systems for fluidic soft actuators. *Int. J. Adv. Robot. Syst.* **15**, 172988141875587 (2018).
43. V. Vallem, Y. Sargolzaeiaval, M. Ozturk, Y. C. Lai, M. D. Dickey, Energy harvesting and storage with soft and stretchable materials. *Adv. Mater.* **33**, e2004832 (2021).
44. R. H. Heisser *et al.*, Valveless microliter combustion for densely packed arrays of powerful soft actuators. *Proc. Natl. Acad. Sci. U.S.A.* **118**, e2106553118 (2021).
45. J. Kim, K. Luo, Z. Suo, A chemical pump that generates high-pressure gas by transmitting liquid fuel against pressure gradient. *Adv. Intell. Syst.* **4**, 2100246 (2022).